FA4869-07-1-4068 (AOARD-07-4068)

Research Final Report

The organic-oxide interfacial layer on the studies of organic electronics (light-emitting diodes and solar cells)

07/01/2007 ~ 06/30/2008

Name of Principal Investigator: Tzung-Fang Guo
E-mail address: guotf@mail.ncku.edu.tw
Institution: Institute of Electro-Optical Science and Engineering, National Cheng Kung University
Mailing address: No. 1 University Road, Tainan 701, Taiwan
Phone: +886-6-2757575 ext. 65284
FAX: +886-6-2747995
Co-investigators (names and institutions): Ten-Chin Wen,
Department of Chemical Engineering, National Cheng Kung University, Tainan 701, Taiwan

Report Documentation Page

Form Approved
OMB No. 0704-0188

1. REPORT DATE	2. REPORT TYPE	3. DATES COVERED
09 OCT 2008	**FInal**	**14-06-2007 to 13-06-2008**

4. TITLE AND SUBTITLE
The organic-oxide interfacial layer on the studies of organic electronic devices

5a. CONTRACT NUMBER
FA48690714068

5b. GRANT NUMBER

5c. PROGRAM ELEMENT NUMBER

6. AUTHOR(S)
Tzung-Fang Guo

5d. PROJECT NUMBER

5e. TASK NUMBER

5f. WORK UNIT NUMBER

7. PERFORMING ORGANIZATION NAME(S) AND ADDRESS(ES)
National Cheng Kung University,No. 1 Univeristy Road,Tainan 701,Taiwan,TW,701

8. PERFORMING ORGANIZATION REPORT NUMBER
N/A

9. SPONSORING/MONITORING AGENCY NAME(S) AND ADDRESS(ES)
AOARD, UNIT 45002, APO, AP, 96337-5002

10. SPONSOR/MONITOR'S ACRONYM(S)
AOARD

11. SPONSOR/MONITOR'S REPORT NUMBER(S)
AOARD-074068

12. DISTRIBUTION/AVAILABILITY STATEMENT
Approved for public release; distribution unlimited

13. SUPPLEMENTARY NOTES

14. ABSTRACT
This project investigated a novel approach to apply an organic-oxide interfacial layer to improve the performance of organic electronic devices, including organic light emitting diodes and organic solar cells.

15. SUBJECT TERMS
Organic Materials, Solar Cells

16. SECURITY CLASSIFICATION OF:			17. LIMITATION OF ABSTRACT	18. NUMBER OF PAGES	19a. NAME OF RESPONSIBLE PERSON
a. REPORT	b. ABSTRACT	c. THIS PAGE			
unclassified	**unclassified**	**unclassified**	**Same as Report (SAR)**	**38**	

Contents

I. Abstract

This research investigates a novel approach to apply an organic-oxide interfacial layer on the studies of organic electronic devices, including ***organic light-emitting diodes*** and ***organic solar cells***. The interfacial reaction at the unique organic-oxide layer/metal junction is investigated by the X-ray photoelectron spectroscopy. The results indicate that the deposition of an Al electrode causes the oxidation at the surface of the light-emissive polymer layer. Introducing an organic-oxide cathode buffer layer suppresses the oxidation and the diffusion of the Al atoms into the functional polymer layer. The formation of a carbide-like (negative carbon) thin layer, which accompanies interfacial interactions, is critical to the injection of electrons through the Al cathode. The balanced charge injection is responsible for the substantially improved device performance. The electroluminescence efficiency of phenyl-substituted poly(para-phenylene vinylene) copolymer-based PLEDs is 0.16 cd/A when Al is used as the device cathode, but is approximately two orders of magnitude higher, 14.53 cd/A, when an organic oxide/Al composite cathode is used. Additionally, the photovoltaic activity of polymer bulk-heterojunction (BHJ) solar cells applying organic oxide/Al complex electrode exhibits the enhanced device performance. Approximate ~4.0 % of power conversion efficiency is achieved in our research team currently for poly(3-hexylthiophene):[6,6]-phenyl C61-butyric acid methyl ester-based polymer solar cells. This part of study is continuing on the project funded by AOARD-08-4076.

II. Technical milestones

- Characterizations and the fundamental studies on the working mechanisms of the organic oxide $(-CH_2CH_2O-)_n$/Al composite nano-structure for O/PLEDs;

Extensive studies had be made by varying the polymer nanolayer with different thickness, functional groups and the metal cathode with different work functions. The specific interfacial reaction between the organic oxide nanolayer with Al during the vacuum thermal deposition is monitored by X-ray photoelectron spectroscopy (XPS). We had identified a new peak positioned at 282.4 eV, which could be attributed to the formation of an Al-C-Oxide complex at the organic-oxide layer/Al junction during the vacuum thermal deposition of Al electrode. Micro raman scattering spectroscopy, Fourier transform infrared spectroscopy, and Atomic force microscopy had be used to characterize

the unique organic-metal properties of the interfacial nanolayer.

- The application of the organic oxide/Al composite electrode for high power conversion efficiency (PCE) polymer bulk-heterojunction (BHJ) solar cells.

The photovoltaic activity of polymer bulk-heterojunction (BHJ) solar cells can be markedly increased by incorporating the organic oxide/Al composite electrode. Currently, ~4.0 % of power conversion efficiency (PCE) is achieved in our research team for BHJ solar cells of P3HT:PCBM (poly(3-hexylthiophene):[6,6]-phenyl C61-butyric acid methyl ester) the derivative of C_{60}) as the active layer. The organic oxide/Al-electrode polymer solar cells have superior characteristics and properties than those of Ca/Al-electrode cells. The interfacial properties at the polymer/metal junction are critical to determine the PCE of polymer BHJ solar cells.

III. Summary of Accomplishments

1. "Organic-oxide cathode buffer layer in fabricating high-performance polymer light-emitting diodes" *Adv. Funct. Mater.* **18**, 3036 (2008). **(AOARD-07-4068)** SCI: 7.496

- Introducing an organic-oxide cathode buffer layer suppresses the oxidation and the diffusion of the Al atoms into the functional polymer layer. The formation of a ***carbide-like (negative carbon) thin layer,*** which accompanies interfacial interactions, is critical to the injection of electrons through the Al cathode.
- The electroluminescence efficiency of phenyl-substituted poly(para-phenylene vinylene) copolymer-based PLEDs is 0.16 cd/A when Al is used as the device cathode, but ***is approximately enhanced by two orders of magnitude***, 14.53 cd/A, when an organic oxide/Al composite cathode is used.

2. "Sulfonated poly(diphenylamine) as a novel hole-collecting layer in polymer photovoltaic cells" *J. Mater. Chem.* **18**, 4478 (2008). **(AOARD-07-4068)** SCI: 4.339

- The sulfonated poly(diphenylamine) (SPDPA) is used as a novel hole collecting layer (HCL) for the studies of polymer photovoltaic (PV) cells.

- P3HT:PCBM-based polymer solar cells have a power conversion efficiency of ***4.2%*** and fill factor of ***0.68*** while SPDPA is used as the HCL. The performance is superior to that of (3.6%, 0.65) PV cells applying commercial poly(3,4-ethylenedioxythiophene):poly(styrenesulfonate) (Baytron AI 4083) as the HCL.
- The hole mobility and the crystallinity of P3HT polymer is improved by the SPDPA placed between the ITO/glass substrate and the active layer, which account for an enhanced device performance.

3. "Effects of film treatment on the performance of poly(3-hexylthiophene)/soluble fullerene-based organic solar cells" *Thin Solid Films* **516**, 3138 (2008). **(AOARD-07-4068)** SCI: 1.693

4. "Modulations of photoinduced magnetoconductance for polymer diodes" *Appl. Phys. Lett.* **92**, 153303 (2008). **(AOARD-07-4068)** SCI: 3.596

IV. Organic-oxide cathode buffer layer in fabricating high-performance polymer light-emitting diodes

Abstract

Spin-casting or thermal evaporation in vacuum of a salt-free, neutral, organic-oxide ultra-thin film as a buffer layer with an aluminum (Al) cathode has become an alternative approach for fabricating high-performance organic and polymer light-emitting diodes (O/PLEDs). [Guo *et al.*, *Appl. Phys. Lett.* **2006**, 88, 113501 and *Appl. Phys. Lett.* **2006**, 89, 053507] The electroluminescence efficiency of phenyl-substituted poly(para-phenylene vinylene) copolymer-based PLEDs is 0.16 cd/A when Al is used as the device cathode, but is approximately two orders of magnitude higher, 14.53 cd/A, when an organic oxide/Al composite cathode is used. The polymer/metal junction in PLEDs with and without depositing an ultra-thin organic oxide interlayer is studied by X-ray photoelectron spectroscopy. Experimental results indicate that the deposition of an Al electrode causes the oxidation at the surface of the light-emissive polymer layer. Introducing an organic-oxide cathode buffer layer suppresses the oxidation and the diffusion of the Al atoms into the functional polymer layer. The formation of a carbide-like (negative carbon) thin layer, which accompanies interfacial interactions, is critical to the injection of electrons through the Al cathode. The balanced charge injection is responsible for the substantially improved device performance. This process is specific to the organic oxide/Al interface, as revealed by a comparison with similar device configurations that have Ag as the electrode, in which no significant interaction in the interface is observed.

Keywords; poly(ethylene oxide), PEGDE, organic oxide, polymer/metal junction, cathode buffer layer

Introduction

Aluminum (Al) is frequently used as electrodes in fabricating organic electronic devices, including organic/polymer light-emitting diodes (O/PLEDs), [1-3] organic photovoltaic or solar cells [4-6] and organic thin-film transistors. [7-9] However, the surface of Al, which intrinsically has a very large amount of non-bonding orbitals (dangling bonds) or surface states, is very active, oxidizing immediately when exposed to the atmosphere and tending to react with organic materials during vacuum thermal evaporation. [10, 11] Additionally, the release of energy of Al followed by the condensation of metallic vapor on the substrate of organic/polymer film at room temperature breaks chemical bonds. Changes in the polymer configuration affect the overall performance of the devices and have stimulated the interest of many researchers. [12-16] Adding a thin layer of the inorganic salts, such as lithium fluoride (LiF) (<1 nm) [3, 17, 18] and cesium carbonate (Cs_2CO_3), [19] ionomers [20] or organic salts that contain Li or calcium (Ca) ions [21, 22] in the cathode interface prevents an unfavorable interaction of Al with the functional organic layer, significantly improving the efficiency of O/PLEDs.

Our recent works have demonstrated a marked improvement in the electroluminescence (EL) efficiency of "high-yellow" phenyl-substituted poly (para-phenylene vinylene) copolymer (HY-PPV)-based PLEDs and tris-(8-hydroxyquinoline) aluminum-based OLEDs using the organic oxide/Al composite cathode. [23-26] Salt ions need not to be added to the cathode buffer layer. [23-29] Introducing a thin layer of ethylene-oxide derivative into the cathode interface of O/PLEDs facilitates the injection of electrons through the Al cathode and inhibits the metal-induced quenching sites of luminescence in the light-emissive layer near the recombination zone. Additionally, the organic oxide film somewhat blocks the excitons from the metal cathode, increasing the probability of radiative recombination. In this work, the interfacial properties at the polymer/metal junction in PLEDs with and without the deposition of an ultra thin organic-oxide interlayer are studied by X-ray photoelectron spectroscopy (XPS). The vacuum thermal deposition of Al is suggested to oxidize the surface of the conjugated polymer, where introducing an ultra-thin (2~5 nm) organic-oxide buffer layer at the polymer/metal junction suppresses the oxidation of the HY-PPV. The formation of a carbide-like layer at the junction interface, which is characterized by the XPS, accompanies the interfacial reaction and is important in facilitating the injection of electrons through the Al electrode. The EL efficiency of PLED made of HY-PPV as the light-emissive layer with Al as the cathode is 0.16 cd/A, but an organic oxide/Al composite cathode increases this value by approximately two orders of

magnitude to 14.53 cd/A. The improved device performance follows essentially the specific interaction of Al with ethylene-oxide groups, $(-CH_2CH_2O-)_n$. When silver (Ag) is used instead of Al with the organic-oxide layer as the electrode, no significant interaction occurs in the polymer/metal junction and no improvement in the device performance is observed.

Experimental Section

Fabrication of PLEDs. The device configuration, as shown in Fig. 1, comprises indium-tin-oxide (ITO)/glass substrate as the anode, poly(3,4-ethylenedioxythiophene):polystyrenesulfonate (PEDOT:PSS Bayer Corp. 4083) as the hole transport layer, HY-PPV film as the light-emissive layer (~850Å), [31] organic-oxide polymer as the interface buffer layer and the metal cathode electrode. The details for the fabrication of typical PLEDs can also be found elsewhere. [24] The organic-oxide film is prepared by thermally evaporating a thin polymer layer of poly(ethylene glycol) dimethyl ether (PEGDE) (Aldrich, Mn ca. 2,000) onto the surface of the HY-PPV film inside a vacuum chamber (10^{-6} torr). The metal electrode is then evaporated on the substrates without breaking the vacuum. The thickness of the thermally evaporated PEGDE and the metal layers are determined by the quartz crystal thickness monitor inside the vacuum chamber. The active pixel area of the device is 0.06 cm^2. The chemical structures of PEGDE and HY-PPV are also presented in Fig. 1.

The current-brightness-voltage and photovoltaic measurement of PLEDs. The current-brightness-voltage (*I-L-V*) measurements are made using a Keithley 2400 source measuring unit and a Keithley 2000 digital multimeter, along with a silicon photodiode, calibrated by a Minolta LS-100 luminosity meter. The photovoltaic measurement is performed under the illumination supplied by a Thermo Oriel 300W solar simulator (AM 1.5G). All of the steps, except for casting the PEDOT:PSS layer, are implemented inside a nitrogen-filled glove box.. The sample configurations of the ITO/PEDOT:PSS/HY-PPV/Al(800Å) (HY-PPV/Al800 device), ITO/PEDOT:PSS/HY-PPV/PEGDE(25Å)/Al(800Å) (HY-PPV/PEGDE25/Al800 device), ITO/PEDOT:PSS/HY-PPV/Ag(800Å) (HY-PPV/Ag800 device) and ITO/PEDOT:PSS/HY-PPV/PEGDE(25Å)/Ag(800Å) (HY-PPV/PEGDE25/Ag800 device) are prepared for the photovoltaic measurement.

XPS measurement. The interfacial properties of the polymer/metal junction is studied by the XPS measurements, which are done by a VG CLAM4 surface analysis system, equipped with an Al Kα radiation (1486.6 eV) at the National Synchrotron Radiation Research Center, Taiwan. The base pressure for the XPS measurement is below

8×10^{-10} Torr and the energy step is 0.025 eV. The sample configurations of the ITO/PEDOT:PSS/HY-PPV (HY-PPV sample), ITO/PEDOT:PSS/HY-PPV/Al(50Å) (HY-PPV/Al50 sample), ITO/PEDOT:PSS/HY-PPV/PEGDE(25Å) (HY-PPV/PEGDE25 sample), ITO/PEDOT:PSS/HY-PPV/PEGDE(25Å)/Al(50Å) (HY-PPV/PEGDE25/Al50 sample), and ITO/PEDOT:PSS/HY-PPV/PEGDE(100Å)/Al(50Å) (HY-PPV/PEGDE100/Al50 sample) are prepared for the XPS measurement. Additionally, Ag is used instead of Al to prepare another set of samples with the identical configurations for the comparison in the XPS measurement. The size of each sample for XPS measurement is around 1.0x1.0 cm^2.

Results and discussion

Figure 2 plots the normalized and corrected C 1s core level spectra from pristine HY-PPV, HY-PPV/Al50, HY-PPV/PEGDE25, HY-PPV/PEGDE25/Al50 and HY-PPV/PEGDE100/Al50 surfaces. The C 1s core level spectrum of the pristine HY-PPV surface has a main peak at a binding energy (BE) of 284.5 eV and a second peak at 286.0 eV. These peaks are associated with hydrocarbon atoms (C-C and C-H) and carbon atoms attached to the oxygen (C-O) of HY-PPV molecules, respectively. The deposition of the Al layer alters the chemical environment of carbon atoms at the surface of HY-PPV polymer, changing the relative intensity and chemical shifts in the spectra (HY-PPV/Al50 sample). However, the deposition of an ultra thin (25 Å) PEGDE layer on the HY-PPV surface has little or no effect on the profile of the C 1s line (HY-PPV/PEGDE25 sample), although the C-C/C-O peak ratio is different for PEGDE and HY-PPV polymers based on the chemical structures as shown in the Fig. 1. The absence of any major change in the XPS spectra can be understood as following from the much lower actual thickness of the PEGDE layer than that of HY-PPV, but the presence of PEGDE in the interface is clearly manifest in the *I-L-V* characteristics of the device.

Figures 3(a)-(d) present deconvolutions of the C 1s core level signals as shown in Fig. 2, based on the minimum Gaussian peaks to yield the best fit after the background subtraction. [32] In Fig. 3(a), peaks #2 (284.5 eV) and #3 (286.0 eV) of the pristine HY-PPV are associated with hydrocarbon atoms (C-C and C-H) and carbon atoms attached to the oxygen (C-O) of HY-PPV molecules, discussed in the above paragraph, respectively. The #4 (287.9 eV) peak is tentatively attributed to C=O bonds and the #5 (288.5 eV) peak is assigned to the carbon atoms in a highly oxidative environment, such as those in carboxylate ester groups. [33-35] The intensity of peaks #4 and #5 in Fig. 3(a) is low, suggesting some unintentional oxidation or contamination of the polymer surface. In

Figs. 3(c) and (d), the #1 (283.1 eV) peak is observed for the HY-PPV films on which had been deposited PEGDE and Al. The binding energies of carbon atoms in this range typically correspond to the carbide-like bonds. [15] The origin or formation of the carbide-like carbons is probably correlated with the interaction between the PEGDE buffer film and Al, as will be discussed below.

In Fig. 3(b), the evaporation of a thin Al layer on an HY-PPV surface changes the relative ratio of the intensities of the deconvoluted peaks and increases the intensity of the high-energy tail in the C 1s core level spectrum above that in Fig. 3(a). The intensity of the #3 peak in Fig. 3(b) is approximately halve, which halving accompanied by a relative increase in the #2 peak (C-C and C-H bond). This result supports the assertion that some C-O bonds at the HY-PPV surface break following the deposition of the Al layer. [36] Furthermore, the marked increase in the intensity of the #5 peak above that in Figs. 3(b) to 3(a), associated with electron-deficient carbons, indicates the oxidation of the conjugated polymer. [33-35] Very likely, many $^{benzene}C\text{-}O\text{-}C^{alkyl}$ groups are transformed to the ester moieties by the addition of the second (carbonyl) oxygen to the C^{alkyl}-atom that is directly attached to the oxo-bridge in the side chain of HY-PPV. As a result, the high electron affinity of oxygen atoms causes a large chemical shift of ~4.0 eV in the C 1s core level spectrum, which is reasonably consistent with the literature. [33, 34] The carbonyl-containing moieties and/or various oxidizing defects in poly(phenylene vinylene) (PPV)-based polymers are known to be the quenching sites for electroluminescence. [37-39] The oxidized interface is also expected to raise the series resistance of the devices, causing the low EL efficiency of PLEDs.

When a thin layer of Al is deposited on the surface of HY-PPV covered with an ultrathin 25Å or 100Å PEGDE layer for XPS measurement, the ~50Å Al metal layer interferes with the penetration of the incident X-rays. The excited photoelectrons that are carried with the C 1s core level signals mainly escape from the PEGDE-rich region located directly beneath the Al layer. The PEGDE film has a higher C-O bond ratio than the HY-PPV film. As a result, in Fig. 3(c), the relative intensity of the #3 peak is higher than that of Fig. 3(a), partially because of the change in the XPS probing depth. The intensity of the #3 peak in Fig. 3(d) is even larger than that in Fig. 3(c) because of the better coverage of the thicker (100Å) PEGDE layer on the HY-PPV surface, as also suggested by a decline in the full-width-half-maximum (FWHM) of the #3 peak in Fig. 3(d). The #5 peak regarding to highly oxidized ester-like carbon species presented in Fig. 3(b) is still observed in Fig. 3(c) and 3(d), suggesting oxidation at the surface of the PEGDE-rich region induced by the deposited Al layer. Noticeably, the #1 peak at 283.1 eV

is observed in both Figs. 3(c) and 3(d), revealing that the formation of a carbide-like thin layer at the interface is accompanied by an interaction between PEGDE and Al. The reaction of the PEGDE layer with the thermally evaporated Al probably suppresses the diffusion of Al into the HY-PPV layer, potentially inhibiting further oxidization or generation of metal-induced EL quenching sites in the HY-PPV layer near the recombination zone. [40-42] Figure 4 schematically presents; (a) the diffusion of Al atoms into the HY-PPV layer during vacuum thermal deposition; (b) the inhibition of diffusion of Al atoms by the PEGDE buffer at the polymer/meal junction.

Figure 5 presents the deconvoluted XPS spectra around the Al 2p peak obtained from the HY-PPV/PEGDE25/Al50 surface. A peak of metallic Al at 71.3 eV with a typically low FWHM is clearly observed in Fig. 5. The broad peak at ~74.0 eV indicates that most Al atoms in the interface are in the form of some undetermined complex with oxygen (Al_xO_y). This result is consistent with the data published in the literature on an ultra-thin Al film that was thermally evaporated on a polymer surface under similar conditions. [11-13] The deconvolution of the Al 2p peak from the HY-PPV/PEGDE25/Al50 surface reveals the presence of two additional peaks - one at 75.4 eV, which corresponds to the oxide species, and the other one at 72.5 eV. The latter peak is at a position that is typically assigned to C-O-Al or C-Al bonds, [11, 43, 44] supporting the formation of carbide-like species revealed by the C 1s spectra in Figs. 3(c) and 3(d).

Devices that were fabricated with the same geometry and under identical conditions, but using Ag rather than Al as the metal electrode, were prepared for comparison. Figure 6 presents the normalized and deconvoluted C 1s core level spectra obtained from HY-PPV/Ag50, HY-PPV/PEGDE25/Ag50, and HY-PPV/PEGDE100/Ag50 surfaces. The best fittings obtained after the deconvolution of the XPS spectra are comprised of only three peaks. The peaks #1 and #5, which correspond to the carbide-like and highly oxidized ester-like carbon species, respectively, as observed in Fig. 3, cannot be extracted in Fig. 6. The ratio of C-C (#2 peak) to C-O (#3 peak) bonds gradually declines from HY-PPV/Ag50, HY-PPV/PEGDE25/Ag50 to HY-PPV/PEGDE100/Ag50, accompanying an increase in PEGDE content. The increase in the area of the #3 peak (C-O) in Figs. 6(b) and 6(c) is substantially larger than that in Figs. 3(c) and 3(d), implying the minimal interaction of the thermally evaporated Ag layer with the polymers (PEGDE and HY-PPV). Additionally, the characteristic Ag 4d doublet in the range of 365~375 eV, commonly used to analyze the chemical shifts in Ag atoms, [35] does not exhibit any variation in the intensity or peak position. (Data not shown herein.) Those results imply that the

carbide-like species are only generated at the PEGDE/Al interface.

The carbide-like (negative carbon) thin layer is essential to the formation of the interfacial dipoles or the decline in the metal work function of the electrode. Figure 7 shows the photovoltaic measurements for HY-PPV/Al800, HY-PPV/PEGDE25/Al800, HY-PPV/Ag800 and HY-PPV/PEGDE25/Ag800 devices. The open-circuit voltages (V_{oc}) of HY-PPV/Al800 and HY-PPV/PEGDE25/Al800 devices were ~1.25 V and ~1.72 V, respectively. This result suggests that the PEGDE buffer layer is responsible for the increase in the built-in potential of the HY-PPV/PEGDE/Al800 device, which implies a drop in the work function of PEGDE/Al cathode or the generation of interfacial dipoles at the polymer/metal junction. [22, 24, 27, 28] However, the V_{oc} of the HY-PPV/PEGDE/Ag800 device is ~0.48 V - even lower than that of the HY-PPV/Ag800 device, ~0.98 V. This result indicates that the PEGDE is most likely an insulating layer, when incorporated with an Ag electrode.

The performance of HY-PPV-based PLED is optimized at a PEGDE buffer layer thickness of 45Å with an Al cathode (HY-PPV/PEGDE45/Al800 device). Figure 8 plots the *I-L-V* curves of HY-PPV/Al800 and HY-PPV/PEGDE45/Al800 devices. The EL intensity of the HY-PPV/PEGDE45/Al800 device exceeds 85,000 cd/m^2 when biased at ~10.0 V. The maximum luminous efficiency is approximately 14.53 cd/A at 6.80V, 7794.02 cd/m^2. However, the EL intensity of the HY-PPV/Al800 device biased at ~10.0 V is only 641.80 cd/m^2 and the maximum luminous efficiency is ~0.16 cd/A at 8.61V, 288.44 cd/m^2. Moreover, the light turn-on voltage of the HY-PPV/PEGDE45/Al800 device was reduced to ~2.50 V from the corresponding value of the HY-PPV/Al800 device, which was about 3.50 V. This result also infers that the voltage for the effective injection of minority carriers was brought forward to the lower electrical bias, in which the shift results from the interfacial dipoles or the decline in the metal work function when the PEGDE buffer layer is introduced at the HY-PPV/Al junction. Figure 9 plots the luminous efficiency versus current density of HY-PPV/Al800 and HY-PPV/PEGDE45/Al800 devices. The luminous efficiency of HY-PPV/PEGDE45/Al800 device (~14.5 cd/A) is about two orders of magnitude higher than that of HY-PPV/Al800 device (~0.16 cd/A) and still remains high and stable when the devices are biased at high current and high brightness regime. Figure 10 displays the EL spectrum of the HY-PPV/PEGDE45/Al800 device. No variation in the EL spectra or the CIE coordinates was observed as the bias was varied. The high EL intensity and luminous efficiency of the HY-PPV/PEGDE45/Al800 device are attributable to the efficient injection of electrons through the cathode and the effective inhibition of the metal-induced EL quenching sites in the HY-PPV layer.

The above findings show that the organic-oxide buffer layer markedly improved the overall device performance. However, further increasing the thickness of the PEGDE interlayer to 100Å degrades the device performance. The series resistance of the device limits the injection of charge carriers through the Al cathode because the PEGDE film is intrinsically insulating. Our earlier publication presented that the device performance changes with the thickness of the PEGDE buffer layer [Guo *et al.*, *Appl. Phys. Lett.* **2006**, 88, 113501].

Conclusion

In summary, the modification of a bare conjugated polymer surface by the thermal deposition of an Al cathode is rather complicated. This study demonstrates the oxidation of both the surface of the conjugated polymer and the Al metallic layer upon the thermal evaporation of Al cathode occurs in a vacuum (10^{-6} torr). The oxidation substantially worsens the performance of PLEDs, but can be suppressed by applying an ultra-thin PEGDE buffer layer at the HY-PPV/Al interface. The polymer/metal junctions of HY-PPV-based PLEDs with and without introducing the PEGDE buffer layer are investigated by the high-resolution XPS. The formation of an ultra-thin Al-C interlayer, which accompanies the interaction of thermally evaporated Al with the PEGDE buffer layer, is presumed to be based on the C 1s and Al 2p core level spectra. The specific organic oxide/Al complex at the cathode interface effectively facilitates the injection of electrons through the Al electrode at a low bias voltage and also suppresses the formation of metal-induced EL quenching sites in the HY-PPV layer. The use of the PEGDE/Al cathode improves the EL intensity and luminous efficiency of HY-PPV-based PLED by approximately two orders of magnitude over those when Al is used as the device cathode. The balanced charge injection and probably the high radiative recombination efficiency in the active layer of HY-PPV/PEGDE45/Al800 device contribute to the enhanced EL efficiency. This work discussed the origins of the functionalized organic-oxide buffer layer in the fabrication of high-performance PLEDs: the steps for preparing the salt-free, neutral interfacial layer can be easily integrated into the manufacturing procedure.

Reference

1. D. Braun, A. J. Heeger, *Appl. Phys. Lett.* **1991**, 58, 1982.
2. C. W. Tang, S. A.VanSlyke, *Appl. Phys. Lett.* **1987**, 51, 913.
3. L. S. Huang, C. W. Tang, M. G. Mason, *Appl. Phys. Lett.* **1997**, 70, 152.
4. H. Hoppe, N. S.Sariciftci, *J. Mater. Chem.* **2006**, 16, 45.
5. C. J. Brabec, N. S. Sariciftci, J. C. Hummelen, *Adv. Funct. Mater.* **2001**, 11, 15.
6. G. Yu, J. Gao, J. C. Hummelen, F. Wudl, A. J. Heeger, *Science*, **1995**, 270, 1789.
7. C. W. Chu, S. H. Li, C. W. Chen, V. Shrotriya, Y. Yang, *Appl. Phys. Lett.* **2005**, 87, 193508.
8. S. H. Li, Z. Xu, L. Ma, C. W. Chu, Y. Yang, *Appl. Phys. Lett.* **2007**, 91, 083507.
9. Guo, T. F.; Tsai, Z. J.; Chen, S. Y.; Wen, T. C.; Chung, C. T. *J. Appl. Phys.* **2007**, 101, 124505.
10. P. Dannetun, M. Logdlund, M. Fahlman, M. Boman, S. Stafstrom, W. R. Salaneck, R. Lazzaroni, C. Fredriksson, J. L. Bredas, S. Graham, R. H. Friend, A. B. Holmes, R. Zamboni, C. Talliani, *Synth. Met.* **1993**, 55, 212.
11. T. P. Nguyen, J. Ip, P. Jolinat, P. Destruel, *Appl. Surf. Sci.* **2001**, 172, 75.
12. W. J. H. van Gennip, J. K. J. van Duren, P. C. Thune, R. A. J. Janssen, J. W. Niemantsverdriet, *J. Chem. Phys*. **2002**, 117, 5031.
13. A. Crispin, A. Jonsson, M. Fahlman, W. R. Salaneck, *J. Chem. Phys.* **2001**, 115, 5252.
14. G. G. Andersson,; W. J. H. van Gennip, J. W. Niemantsverdriet, H. H. Brongersma, *Chem. Phys.* **2002**, 278, 159.
15. R. Sutcliffe, W. W. Lee, J. F. Gaynor, J. D. Luttmer, D. Martini, J. Kelber, M. A. Plano, *Appl. Surf. Sci.* **1998**, 126, 43.
16. L. Sandrin, E. Sacher, *Appl. Surf. Sci.* **1998**, 135, 339.
17. G. E. Jabbour, Y. Kawabe, S. E. Shaheen, J. F. Wang, M. M. Morrell, B. Kippelen, N. Peyghambarian, *Appl. Phys. Lett.* **1997**, 71, 1762.
18. J. Yoon, J. J. Kim, T. W. Lee, O. O. Park, *Appl. Phys. Lett.* **2000**, 76, 2152.
19. J. Huang, Z. Xu, Y. Yang, *Adv. Funct. Mater.* **2007**, 17, 1966.
20. T. W. Lee, O. O. Park, L. M. Do, T. Zyung, T. Ahn, H. K. Shim, *J. Appl. Phys.* **2001**, 90, 2128.
21. Y. Cao, G. Yu, A. J. Heeger, *Adv. Mater.* **1998,** 10, 917.
22. Q. Xu, J. Ouyang, Y. Yang, T. Ito, J. Kido, *Appl. Phys. Lett.* **2003**, 83, 4695.
23. T. F. Guo, F. S. Yang, Z. J. Tsai, T. C. Wen, S. N. Hsieh, Y. S. Fu, *Appl. Phys. Lett.* **2005**, 87, 013504.
24. T. F. Guo, F. S. Yang, Z. J. Tsai, T. C. Wen, S. N. Hsieh, Y. S. Fu, C. T. Chung, *Appl. Phys. Lett.* **2006**, 88, 113501.

25. T. F. Guo, F. S. Yang, Z. J. Tsai, G. W. Feng, T. C. Wen, S. N. Hsieh, C. T. Chung, C. I. Wu, *Appl. Phys. Lett.* **2006**, 89, 051103.
26. T. F. Guo, F. S. Yang, Z. J. Tsai, T. C. Wen, C. I. Wu, C. T. Chung, *Appl. Phys. Lett.* **2006**, 89, 053507.
27. X. Y. Deng, W. M. Lau, K. Y. Wong, K. H. Low, H. F. Chow, Y. Cao, *Appl. Phys. Lett.* **2004**, 84, 3522.
28. Y. H. Niu, H. Ma, Q. Xu, A. K. Y. Jen, *Appl. Phys. Lett.* **2005**, 86, 083504.
29. J. H. Park, O. O. Park, J. W. Yu, J. K. Kim, Y. C. Kim, *Appl. Phys. Lett.* **2004**, 84, 1783.
30. K. Cho, S. W. Cho, C. N. Whang, K. Jeong, S. J. Kang, Y. Yi, *Appl. Phys. Lett.* **2007**, 91, 152107.
31. H. Becker, H. Spreitzer, W. Kreuder, E. Kluge, H. Schenk, I. Parker, Y. Cao, *Adv. Mater.* **2000**, 12, 42.
32. G. L. Pakhomov, L. G. Pakhomov, V. I. Shashkin, J. M. Tura, J. M. Ribo, L. Ottaviano, *Nucl. Instr. and Meth. in Phys. Res. B*, **2002**, 194, 269.
33. C. C. Wang, G. H. Hsiue, *J. Polymer Sci. Pt. A*, **1993**, 31, 2601.
34. M. Atreya, S. Li, E. T. Kang, K. G. Neoh, K. L. Tan, *Polymer Degradation and Stability*, **1999**, 63, 53.
35. N. Dam, M. M. Beerbom, J. C. Braunagel, R. Schlaf, *J. Appl. Phys.* **2005**, 97, 024909.
36. K. Konstadinidis, F. Papadimitrakopoulos, M. Galvin, R. L. Opila, *J. Appl. Phys.* **1995**, 77, 5642.
37. M. Yan, L. J. Rothberg, F. Papadimitrakopoulos, M. E. Galvin, T. M. Miller, *Phys. Rev. Lett.*, **1994**, 73, 744.
38. R. H. Friend, R. W. Gymer, A. B. Holmes, J. H. Burroughes, R. N. Marks, C. Taliani, D. D. C. Bradley, D. A. Dos Santos, J. L. Brédas, M. Lögdlund, W. R. Salaneck, *Nature*, **1999**, 397, 121.
39. D. R. Baigent, A. B. Holmes, S. C. Moratti, R. H. Friend, *Synth. Met.* **1996**, 80, 119.
40. H. Becker, A. Lux, A. B. Holmes, R. H. Friend, *Synth. Met.* **1997**, 85, 1289.
41. H. Becker, S. E. Burns, R. H. Friend, *Phys. Rev. B*, **1997**, 56, 1893.
42. P. W. M. Blom, M. C. J. M. Vissenberg, J. N. Huiberts, H. C. F. Martens, H. F. M. Schoo, *Appl. Phys. Lett.* **2000**, 77, 2057.
43. T. P. Nguyen, J. L. Mansot, *Thin Solid Films*, **1996**, 283, 135.
44. S. J. Ding, Q. Q. Zhang, D. W. Zhang, J. T. Wang, Y. D. Zhou, W. W. Lee, *Appl. Surf. Sci.* **2001**, 178, 140.

Figure Captions

FIG. 1. The chemical structure of PEGDE and HY-PPV, and the configuration of PLED presented in this study.

FIG. 2. The normalized and corrected C 1s core level spectra obtained from (○) pristine HY-PPV, (□) HY-PPV/Al50, (◇) HY-PPV/PEGDE25, (△) HY-PPV/PEGDE25/Al50, and (■)HY-PPV/PEGDE100/Al50 surfaces.

FIG. 3. The deconvolutions of the normalized and corrected C 1s core level signals from (a) HY-PPV, (b) HY-PPV/Al50, (c) HY-PPV/PEGDE25/Al50, and (d) HY-PPV/PEGDE100/Al50 surfaces.

FIG. 4. A schematic plot presents; (a) the diffusion of Al atoms into the HY-PPV layer during vacuum thermal deposition; (b) the inhibition of diffusion of Al atoms by the PEGDE buffer at the polymer/meal junction. The "cleaner" excitons recombination zone is expected in (b).

FIG. 5. The deconvolution of the normalized and corrected Al 2p peak obtained from HY-PPV/PEGDE25/Al50 surface.

FIG. 6. The deconvolution of the normalized and corrected C 1s core level spectra obtained from (a) HY-PPV/Ag50, (b) HY-PPV/PEGDE25/Ag50, and (c) HY-PPV/PEGDE100/Ag50 surfaces.

FIG. 7. The photovoltaic measurements of (□) HY-PPV/Al800, (△) HY-PPV/PEGDE25/Al800, (◆) HY-PPV/Ag800, and (▼) HY-PPV/PEGDE25/Ag800 devices.

FIG. 8. *I-L-V* curves of (□) HY-PPV/Al800 and (●) HY-PPV/PEGDE45/Al800 devices.

FIG. 9. The luminous efficiency versus current density of (□) HY-PPV/Al800 and (●) HY-PPV/PEGDE45/Al800 devices.

FIG. 10. EL spectrum of HY-PPV/PEGDE45/Al800 device. No variation in the EL spectra or the CIE coordinates was observed at varied bias conditions.

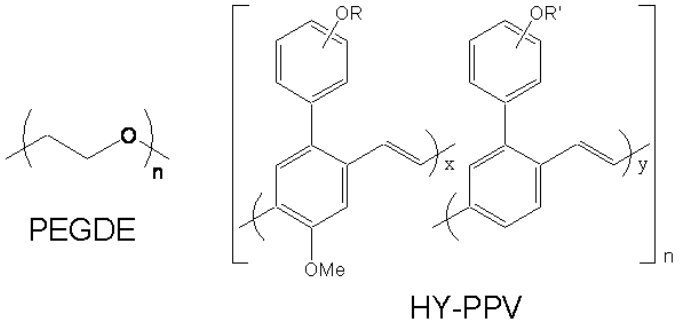

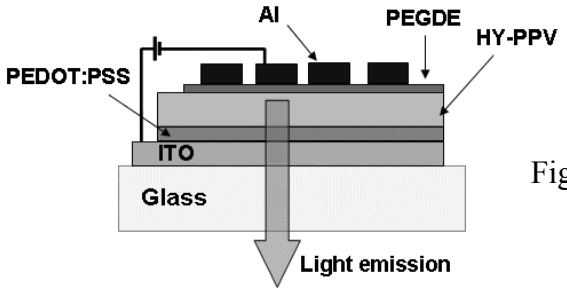

Figure 1

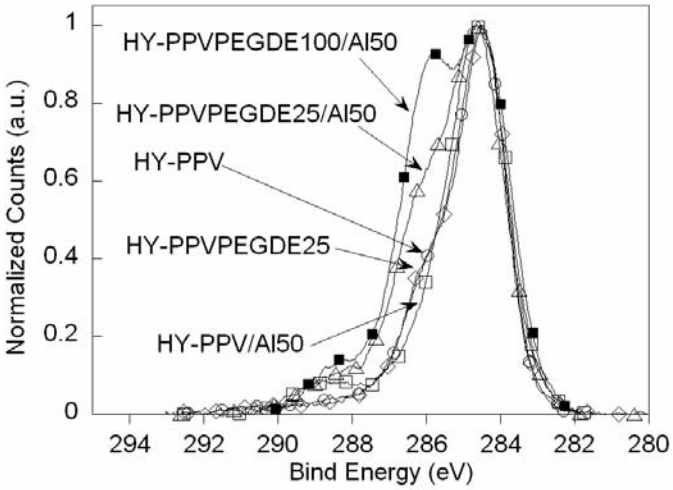

Figure 2

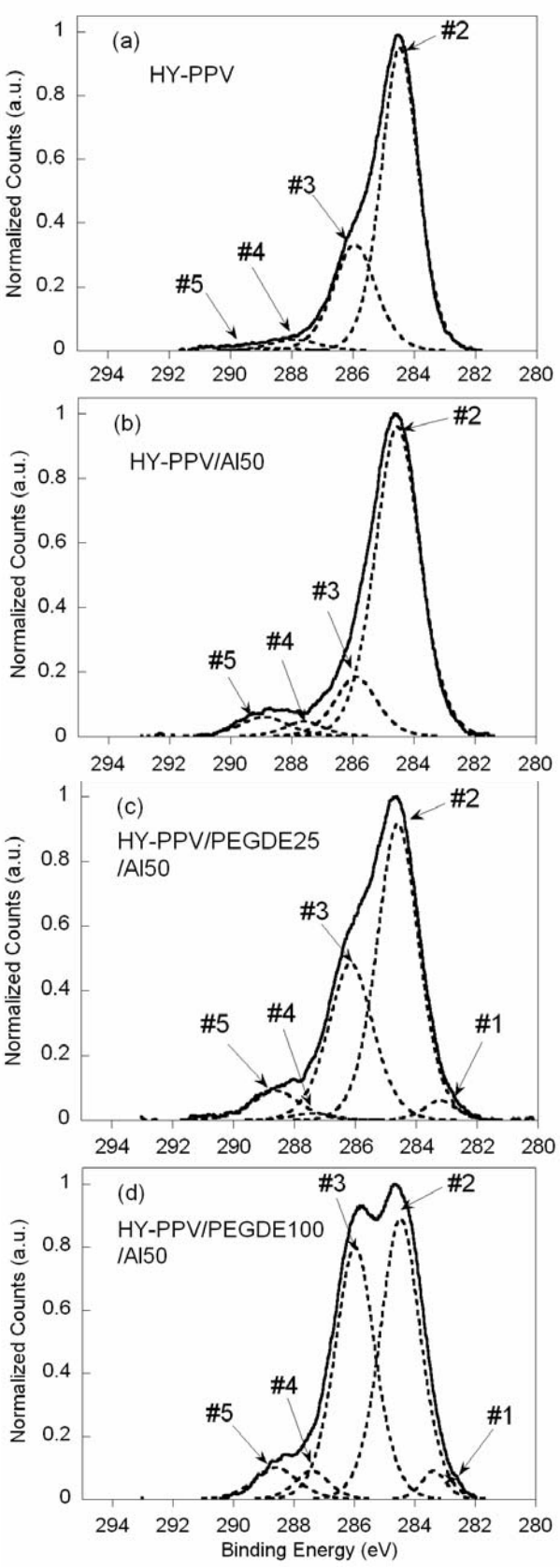
(a)
HY-PPV
(b)
HY-PPV/Al50
(c)
HY-PPV/PEGDE25
/Al50
(d)
HY-PPV/PEGDE100
/Al50
#1
#2
#3
#4
#5
Normalized Counts (a.u.)
Binding Energy (eV)
0
0.2
0.4
0.6
0.8
1
280
282
284
286
288
290
292
294

Figure 3

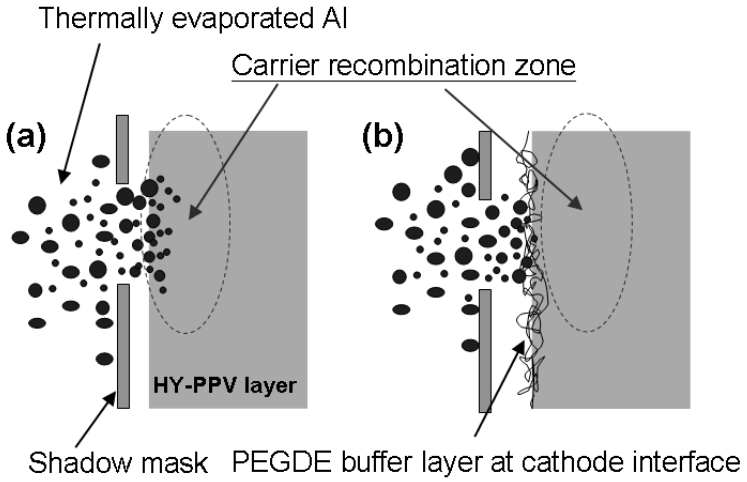

Figure 4

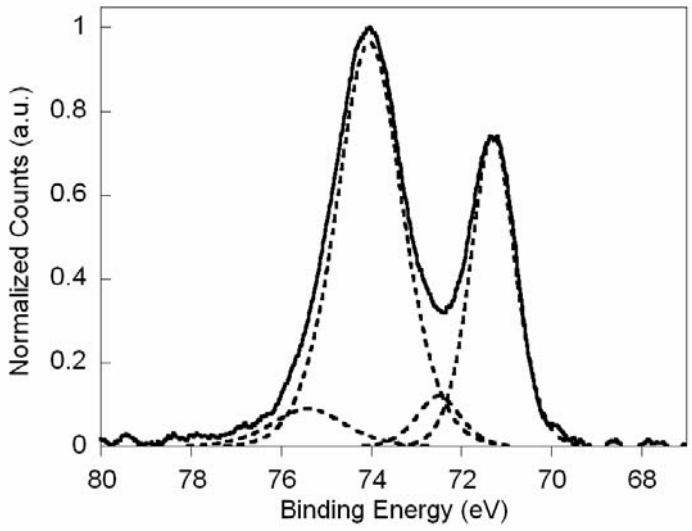

Figure 5

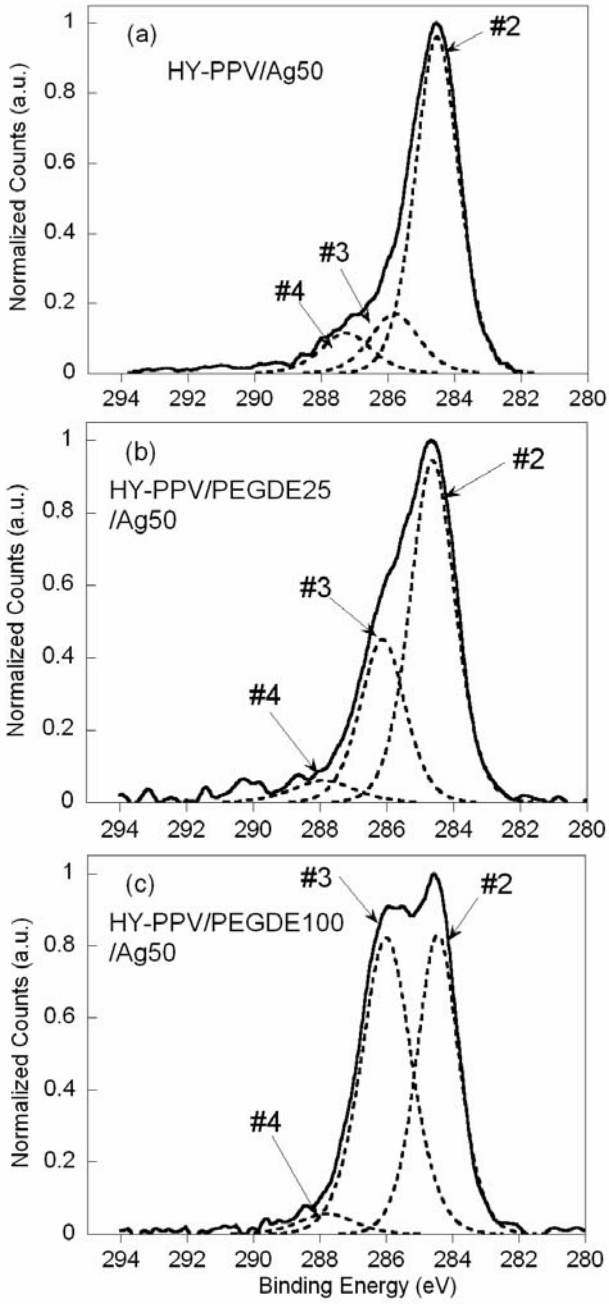
(a)
HY-PPV/Ag50
#2
#3
#4
(b)
HY-PPV/PEGDE25
/Ag50
#2
#3
#4
(c)
HY-PPV/PEGDE100
/Ag50
#3
#2
#4
Normalized Counts (a.u.)
Binding Energy (eV)
0
0.2
0.4
0.6
0.8
1
294
292
290
288
286
284
282
280

Figure 6

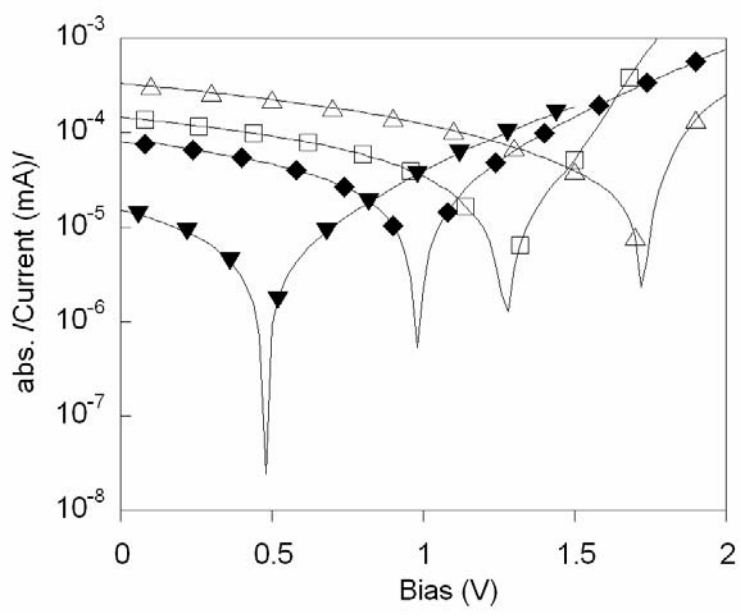

Figure 7

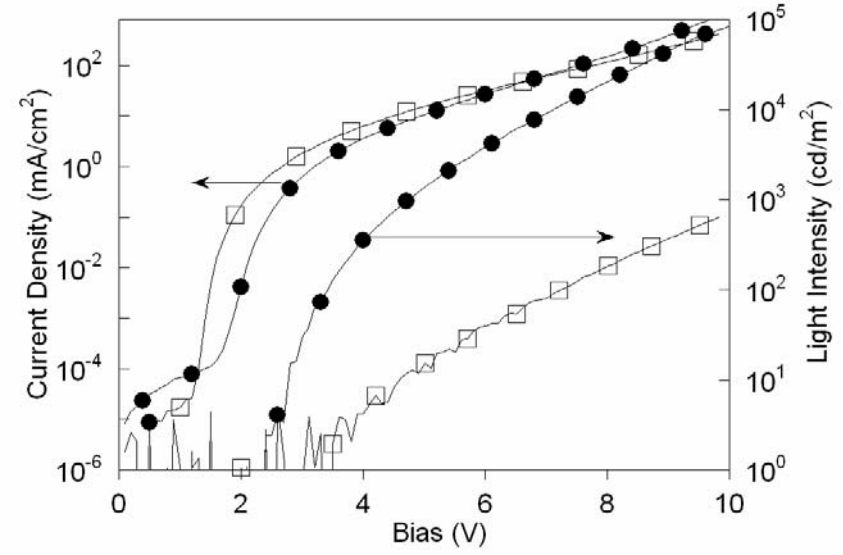

Figure 8

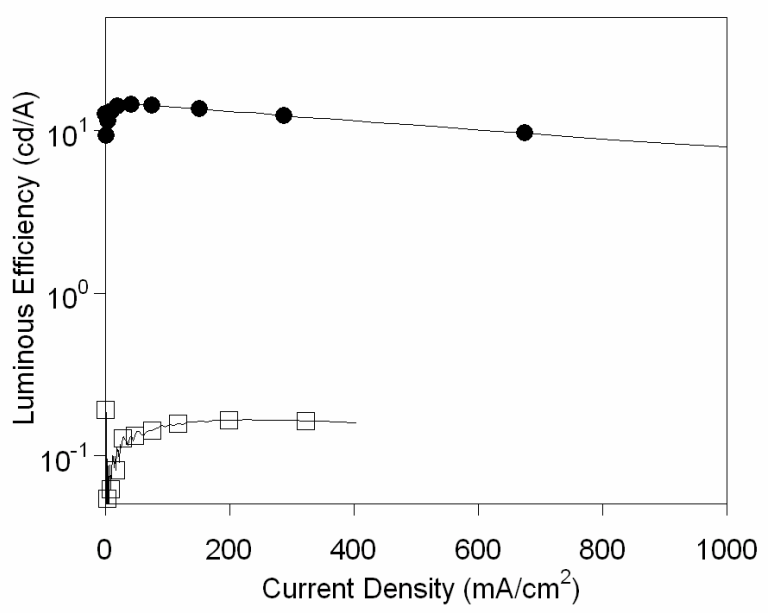

Figure 9

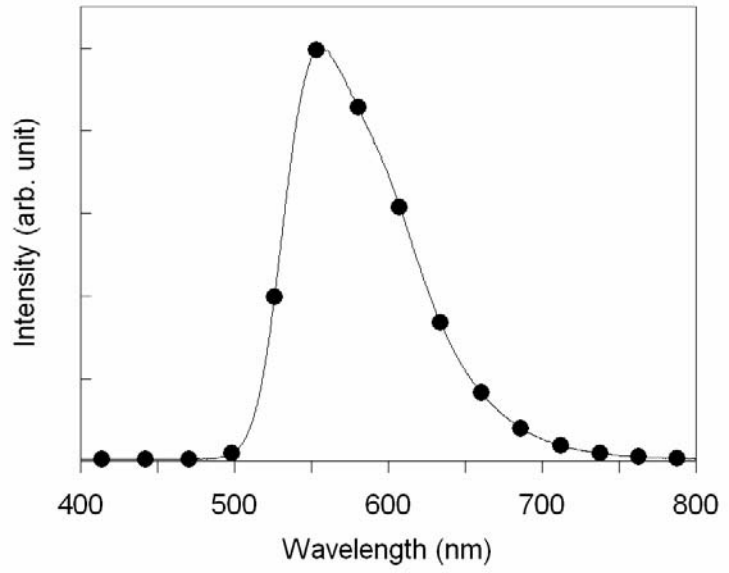

Figure 10

V. Sulfonated poly(diphenylamine) as a novel hole-collecting layer in polymer photovoltaic cells

Abstract

This work applies sulfonated poly(diphenylamine) (SPDPA) as a novel hole collecting layer (HCL) for the studies of polymer photovoltaic (PV) cells. PV cell of poly(3-hexylthiophene) (P3HT):[6,6]-phenyl C_{61} butyric acid methyl ester as the active layer based on SPDPA as HCL possessed the better power conversion efficiency (4.2%) and fill factor (0.68) than that on the commercial poly(3,4-ethylenedioxythiophene):poly(styrenesulfonate) (Baytron AI 4083) (3.6% and 0.65). The morphology change of active layer is observed by the atomic force microscopy and grazing-incidence X-ray diffraction. The hole-only device is fabricated to measure hole injection current and hole mobility, which supports the increased crystallinity of P3HT with SPDPA as HCL. The enhanced device performance is attributed to the improved hole mobility and the increased crystallinity of P3HT due to specific properties of SPDPA.

Introduction

Polymer photovoltaic (PV) cells offer tremendous potential for renewable, alternative source of energy due to flexible, light-weight, and inexpensive advantages. Among these, poly(3-hexylthiophene) (P3HT) and [6,6]-phenyl C_{61} butyric acid methyl ester (PCBM) blending system is the most interesting one because of the fast progress from several reputed groups. The power conversion efficiency (PCE) has been enhanced to 4-5% through the blends treated such as thermally annealing[1-2], slow drying[3] and adding surfactant into active layer[4], which induced the increase in polymer crystallinity. Besides, high PCEs of more than 6% were achieved by fabricating tandem cell architecture, where two devices with different absorption characteristics are linked to utilize a wider range of the solar spectrum[5].

Except for controlling the morphology of polymer composites, PCE could be raised by applying the appropriate electrodes. For example, LiF/Al6 or Ca/Al7 can be used as electron collecting layer to improve the open-circuit voltage (V_{oc}) and fill factor (*FF*) of PV cells. The LUMO levels of acceptor would pin the Fermi levels of contact electrode, which results in the band bending and reducing the interfacial barrier resistance. Recently, polymeric material poly(ethylene oxide) as electron collecting electrode was reported being able to increase V_{oc} in PV cells[8]. On the other hand, the commercial poly(3,4-ethylenedioxythiophene): poly(styrenesulfonate) (PEDOT:PSS) has always been used as hole collecting layer (HCL). Ko *et al*. improved the conductivity of PEDOT:PSS by utilizing mannitol[9]. Simultaneously, the enhanced short circuit current density (J_{sc}) and PCE could be observed due to the reduction of the series resistance (R_s). In any event, related literatures indicated that the buffer layers in organic or polymer electronic devices played a significant role to control the carrier transport or collection. Besides, HCL may influence the arrangement of active layer due to its interfacial interaction. In the case of organic field effect transistor, the molecular orientation of P3HT was controlled by various functional groups of self-assembled monolayers due to the difference of intermolecular interaction between P3HT and subtrate[10]. The different surface treatment, converting the hydrophilic surface to hydrophobic surface, would probably improve the surface roughness, orientation and crystallinity of P3HT film.

Herein, we reported a novel hole collecting layer, sulfonated poly(diphenylamine) (SPDPA), with high transmittance (near 80% transmittance in visible region) and appropriate work function (~5.24eV). Due to the specifics of chemical structure, polarity, and surface energy, SPDPA layer would assist in the crystallinity of P3HT in the active layer during the spin-coating and film-growing process, resulting in the enhanced PCE.

Experimental section

The novel hole collecting layer, SPDPA, was synthesized by a oxidative polymerization coupled with a facile sulfonation process. The detailed preparation procedure and characterization can be referred to our previous work[11]. The commercial PEDOT:PSS (Baytron-P AI 4083) was utilized as contrast HCL.The chemical structure of SPDPA and PEDOT:PSS are shown in scheme 1 for comparison.

PV cells were fabricated by coating the active layer of P3HT:PCBM which sandwiched between hole collecting electrode, a transparent ITO (received from RITEK Corp., 15 Ω/□)/HCL, and electron collecting electrode, Calcium (Ca) (40 nm)/ Aluminum (Al) (100 nm). In the hole-only device, the Gold (Au) (30 nm) and Silver (Ag) (100 nm) were also thermally deposited onto the P3HT:PCBM film as top electrode. The active area of device was 0.08 cm^2. Before device fabrication, the ITO glass substrates were cleaned by ultrasonic treatment in detergent, deionized water, acetone and isopropyl alcohol sequentially. The hole collection layers of PEDOT:PSS and SPDPA (the concentration of 1.2 wt.-% in deionized water) were spin-coated to modify the ITO surface. After baking at 150 □ for 30 min, the substrates were transferred to a nitrogen-filled glove box. P3HT (Nano-c) and PCBM (Nano-c) have ratio 1:1 with a concentration of 2 wt.-% in 1,2-dichlorobenzene. The blend was stirred for at least 24 hr at room temperature in the glove box. The active layer was spin coated at 650 rpm for 60 s and then transferred to the sealed glass petri dish to carry out solvent annealing procedure as described in Ref. 3 (denoted as slow-grown film). Besides, the fast-grown film was spin coated at 1200 rpm for 60 s, which was investigated surface morphology by Atomic force microscopy (AFM). In order to avoid the morphological change upon heat annealing, the device is free of baking treatment. The current density -voltage (*J-V)* characteristics of devices were measured with keithley 2400 source-measure unit under simulated AM 1.5G irradiation (100 $mWcm^{-2}$) using an Oriel 91160A 300W Solar Simulator in glove box. The illumination intensity used was calibrated by standard Si photodiode detector with KG-5 color filter (Hamamastsu, S1133)[12]. The incident photon-to-electron conversion efficiency (IPCE) spectra were measured with a lock-in preamplifier (SR510, Standard Research Systems) after illuminating the devices with monochromatic light from xenon lamp (Oriel 66902 150 mW Solar Simulator) passing through a monochromator (Oriel Cornerstone 130TM 1/8m monochromator). The spectral response was normalized by standard mono-silicon solar cell before processing IPCE experiment.

The surface energy of PEDOT:PSS and SPDPA was determined through

Owens-Wendt contact angle measurements using water and diiodomethane as probe liquids[13] and the work functions were measured by a Riken Keiki AC-2 photoelectron spectroscopy in air. The measurement of conductivity was carried out by four-point probe experiment. Transmittance spectra were analyzed with a UV-visible spectrometer constructed by GBC Scientific Equipment, Australia (model GBC Cintra 10e). AFM was performed with a NanoScope □a (Digital Instruments Inc.) run in the tapping mode. The synchrotron grazing-incidence X-ray diffraction (GI-XRD) measurements were performed at 17B1 beamline (wavelength ~ 1.37 Å) of National Synchrotron Radiation Research Center in Taiwan. The grazing incidence angle is fixed in 0.18°. The measurement of the thickness was made by a Tencor Alpha-Step 500 Surface profiler.

Results and discussions

The device performance of PV cells is persuaded by Jsc, Voc and FF while these parameters are directly determined by overall device resistance, including intrinsic conductivity of collecting layer, barrier height at interface and the carrier mobility of active layer. Accordingly, the corresponding data of polymeric characteristics are listed in Table 1. The work function of SPDPA (5.24eV) and PEDOT:PSS (5.07eV) is higher than HOMO of P3HT (4.9eV). It implies that both cases can avoid unnecessary interfacial barrier and meanwhile the former is superior to the latter. Besides, the morphology of active layer could be affected by the surface energy and polarity of bottom layer upon annealing process[14,15], so the contact angle and surface energy experiment were also examined. The small contact angle and high surface energy of SPDPA are attributable to its hydrophilic property because of NH and SO_3H groups (one SO_3H group attached to every phenyl rings) on its polymer chain. The high conductivity of HCL is also an important factor to avoid transporting bottleneck in hole collecting electrode. Unfortunately, SPDPA has the lower conductivity than PEDOT:PSS. To circumvent the above drawback, the thickness of SPDPA layer can be reduced for the optimal resistance.

The Figures 1(a) and 1(b) show current density-voltage (*J*-*V*) behaviors of PV cells under illumination and dark, respectively. At first under dark, there is the same order of magnitude for leakage current and rectification of PV cells based on PEDOT:PSS and SPDPA with various thicknesses. It indicates that both SPDPA and PEDOT:PSS provide good modification and buffer function. The thickness of SPDPA is controlled at ca. 26 nm, 14 nm and 10 nm, respectively, by various spin-coating rates of 1500, 3500 and 5500 rpm. Under illumination, all PV cells have almost the same V_{oc} (0.60 V), being attributed to the Ohmic contact effect between P3HT and HCLs, which was reported by Mihailetchi *et al*[7].

In our case, V_{oc} is accordingly determined by the molecular energy difference between the donor HOMO and the acceptor LUMO. For the convenience of further discussion, all performance parameters derived from Figure 1 are listed in Table 2. Surprisingly, both J_{sc} and PCE progressively increase with decreasing SPDPA thickness. The device based on SPDPA (10 nm) can achieve 4.2% PCE, which obviously exceeds 3.6% based on PEDOT:PSS. On the contrary, less J_{sc} was collected from the device based on 26 nm SPDPA than PEDOT:PSS, being attributable to the lower conductivity of SPDPA. For a comparison, the device based on 10 nm PEDOT:PSS were also fabricated and the corresponding data was summarized in Table 2. Although thickness of PEDOT:PSS was diminished for avoiding the hole transporting obstruction, the device performance was no significantly enhanced. The series resistance (*Rs*) including the resistance of active layer, metal-organic contacts, and the resistance of collecting electrode represents the Ohmic loss, significantly affecting the device performance[9]. Here, the data of *Rs* were calculated from *J-V* curves under dark (Figure 1(b)). The *Rs* also decreases with decreasing SPDPA thickness. The *Rs* of the device based on 10 nm SPDPA is much smaller than that on PEDOT:PSS (both 10 nm and 30 nm PEDOT:PSS), being favorable for charge transporting in this device. Besides, *FF* increases to 0.68 with decreasing thickness to 10 nm, implying that the electron-hole pairs are more equally separated and transported to collecting electrodes in this case. In the P3HT:PCBM device, hole mobility is smaller than electron mobility. The improvement of hole mobility containing balances separation efficiency and consequently reduce the space charge effect. The above results will accord with the increased FF. It seems that 10 nm SPDPA as HCL does improve FF and hole mobility.

For the further discussion, IPCE and transmittance spectra of HCL are measured and shown in Figure 2. Both PEDOT:PSS and SPDPA coated on ITO possess ca. 86% transmittance between 450 nm and 750 nm wavelength. There existed the stronger absorption in the range of 350 nm to 450 nm for SPDPA than PEDOT:PSS due toπ-π* transition of benziod ring. IPCE spectra of devices based on PEDOT:PSS and SPDPA show similar curves although the slightly low transmittance of SPDPA in this specific region could consume some incident photon. The maximum IPCE reaches ca. 65.2 % and 58.8 % for the devices based on 10 nm SPDPA and PEDOT:PSS, respectively. It is consistent with the data of Jsc under simulating AM 1.5G irradiation.

It is interesting that the device based on 10nm SPDPA possesses 4.2% PCE with high value FF at 0.68, being attributable to the higher hole transporting property than PEDOT:PSS. Related literatures indicate interfacial interaction can influence molecular

arrangement upon casting film[10,16]. Figure 3 shows Atomic force microscopy (AFM) height images for observing the surface of P3HT:PCBM coated on PEDOT:PSS and SPDPA via solvent annealing process. A very thin film has been also prepared by spin-coating at 1200 rpm to observe the morphology of active layer relatively near HCL (denoted as fast-grown film). In order to circumvent the bottom layer roughness, the surface roughness of SPDPA and PEDOT:PSS coated on ITO was ascertained to be the same (Table 1). For P3HT:PCBM film on PEDOT:PSS, the root mean square (rms) roughness of fast-grown film and slow-grown film is 1.12 nm and 8.07 nm, respectively. The surface roughness enlarges via solvent annealing process due to the presence of polymer self-organization. Similarly, more rough surface was observed in slow-grown film (rms~12.61 nm) than fast-grown film (rms~1.78 nm) for P3HT:PCBM on SPDPA. Meanwhile, the surface roughness is larger on SPDPA than PEDOT:PSS. Regarding coarse surface roughness, some reports considered the existence of interfacial area for charge separation[1] or high crystallinity within two phase networks[4].AFM image practically investigate the surface morphology of the film, being unable to determine the structure of active layer. Therefore, the synchrotron grazing-incidence X-ray diffraction (GI-XRD) measurement is proposed to support the above speculation and while grazing incidence is fixed at very small angle in order to observe the same basis of thickness. Figure 4 shows XRD patterns for the microstructural crystallinity of P3HT:PCBM based on PEDOT and SPDPA. Clearly, the stronger intensity of both (100) and (200) reflection peaks belonging to P3HT domination of a-axis orientation (indicating main chain parallel and side chain perpendicular to the substrate) can be obtained on SPDPA sample than PEDOT:PSS sample, definitely conforming our presumption. It is interesting to realize why the different degrees of crystallinity are observed when P3HT:PCBM is coated on PEDOT:PSS or SPDPA. The P3HT unmixed with PCBM would like to orientate perpendicular to the bottom layer which possesses strong polar groups because the interface is subject to repulaive force between the pi-electron clouds of the thienyl backbone[10]. In the case of P3HT:PCBM, it spontaneously forms crystallite toward a-axis orientation rather than other axis orientation (such as b-axis or c-axis) upon annealing treatment[14]. It is considered that SPDPA with strong polarity could assist active layer in arrangement of a-axis orientation. On the other hand, the high surface energy of SPDPA prompts P3HT:PCBM to instant adhesion and orientation, being observed in fast-grown film. As P3HT:PCBM near interface is guided by SPDPA toward more order orientation, layer-by-layer film would be favorable to self-prganizing into highly ordered lamellar architecture. Thus, the overall active layer enhances crystallinity.

From the above discussion of roughness and crystallinity of P3HT on SPDPA, we presume the hole mobility is enhanced. In order to cross-check this presumption, we fabricated hole-only devices as following structure: ITO/HCL/P3HT:PCBM/ Au/Ag. The J-V curves of the hole-only devices are shown in Figure 5. Here, we correct voltage (V_{appl}) with build-in potential (V_{bi}) by $V=V_{appl}-V_{bi}$. The device based on SPDPA exhibits the more current density than that on PEDOT:PSS at the same operating voltage, confirming the enhancement of hole mobility by SPDPA. Futher, the curves are fitted by SCLC model at low bias for calculating hole mobility[17]. The calculation is followed by $J= 9\varepsilon_0\varepsilon_r\mu V^2/8L^3$, where $\varepsilon_0\varepsilon_r$ is the permittivity of the polymer, μ is the carrier mobility and L is the device thickness. The higher hole mobility can be calculated in the device based on SPDPA (1.55×10^{-7} $m^2V^{-1}s^{-1}$) than PEDOT:PSS (1.36×10^{-7} $m^2V^{-1}s^{-1}$). It steadily confirms our presumption that the high PCE of the device based on 10 nm SPDPA is attributed to the increased crystallinity P3HT and the enhanced hole mobility.

Conclusions

We have a successful demonstration using SPDPA as HCL in polymer PV cells. The better device performances including 4.2% PCE, 0.68 FF, and 65.2% IPCE can be found in the device based on 10 nm SPDPA than PEDOT:PSS as HCL. The role of 10 nm SPDPA is used to obtain the high crystallinity of P3HT; to enhance the hole mobility; to reduce the series resistance; and to have the Ohmic contact between HCL and P3HT. This successful demonstration will stimulate wide studies of polymer PV cells with the inverted structure because SPDPA can be well dissolved in other organic polar solvents.

Reference

1. W. L. Ma, C. Y. Yang, X. Gong, K. Lee and A. J. Heeger, *Adv. Funct. Mater.* **2005**, *15*, 1617.
2. M. Reyes-Reyes, K. Kim and D. L. Carroll, *Appl. Phys. Lett.* **2005**, *87*, 083506.
3. G. Li, V. Shrotriya, J. S. Huang, Y. Yao, T. Moriarty, K. Emery and Y. Yang, *Nat. Mater.* **2005**, *4*, 864.
4. W. Wang, H. B. Wu, C. Y. Yang, C. Luo, Y. Zhang, J. W. Chen and Y. Cao, *Appl. Phys. Lett.* **2007**, *90*, 183512.
5. J. Y. Kim, K. H. Lee, N. E. Coates, D. Moses, T. Q. Nguyen, M. Dante and A. J. Heeger, *Science*, **2007**, *317*, 222.
6. C. J. Brabec, S. E. Shaheen, C. Winder, S. Sariciftci and P. Denk, *Appl. Phys. Lett.* **2002**, *80*, 1288.
7. V. D. Mihailetchi, P. W. M. Blom, J. C. Hummeien and M. T. Rispens, *J. Appl. Phys.* **2003**, *94*, 6849.
8. F. Zhang, M. Ceder and O. Inganas, *Adv. Mater.* **2007**, *19*, 1835.
9. C. J. Ko, Y. K. Lin, F. C. Chen and C. W. Chu, *Appl. Phys. Lett.* **2007**, *90*, 063509.
10. D. H. Kim, Y. D. Park, Y. Jang, H. Y, Y. H. Kim, J. I. Han, D. G. Moon, S. Park, T. Chuang, C. Chang, M. Joo and C. Y. Ryu, *Adv. Funct. Mater.* **2005**, *15*, 77.
11. C. Y. Li, T. C. Wen, T. F. Guo, S. S. Hou, *Polymer*, **2008**, *49*, 957.
12. V. Shrotriya, G. Li, Y. Yao, T. Moriarty, K. Emery, Y. Yang, *Adv. Funct. Mater.* **2006**, *16*, 2016.
13. M. Zenkiewicz, *Polym. Test.* **2007**, *26*, 14.
14. J. S. Kim, J. H. Park, J. H. Lee, J. Jo, D. Y. Kim and K. Cho, *Appl. Phys. Lett.* **2007**, *91*, 112111.
15. M. Campoy-Quiles, T. Ferenczi, T. Agostinelli, P. G. Etchegoin, Y. K. Kim, T. D. Anthopoulos, P. N. Stavrinou, D. D. C. Bradley and J. Nelson, *Nat. Mater.* **2007**, *7*. 158.
16. R. J. Kline, M. D. Mcgehee and M. F. Toney *Nat. Mater.* **2006**, *5*. 222.
17. V. Shrotriya, Y. Yao, G. Li and Y. Yang, *Appl. Phys. Lett.* **2006**, *89*, 063505.

Table 1. Polymeric surface characteristics and roughness for the various hole conductor layers.

Material	Work function (eV)[a]	Conductivity (S/cm)[b]	Contact angle (°) Water	Diiodomethane	Surface energy (mJ/m^2)	Surface roughness (nm)
PEDOT	5.07	8.3×10^{-4}	21.6	29.4	68.5	0.94
SPDPA	5.24	1.1×10^{-4}	□10	19.8	72.7	0.91

a. Measured from the AC-2 photoelectron spectroscopy.

b. Measured from the four-point probe.

Table 2. The device performance for various hole conductor layers.

Material	V_{oc} (V)	J_{sc} (mA/cm^2)	FF	PCE (%)	Rs[c] ($\Omega\ cm^2$)
PEDOT 4000 rpm (30 nm)	0.60	9.23	0.65	3.6	3.03
PEDOT 8000 rpm (10 nm)	0.60	9.39	0.66	3.7	2.35
SPDPA 1500 rpm (26 nm)	0.60	8.96	0.65	3.5	3.31
SPDPA 3500 rpm (14 nm)	0.58	10.21	0.66	3.9	2.47
SPDPA 5500 rpm (10 nm)	0.60	10.33	0.68	4.2	1.93

c. Calculated by the J-V curves in the dark.

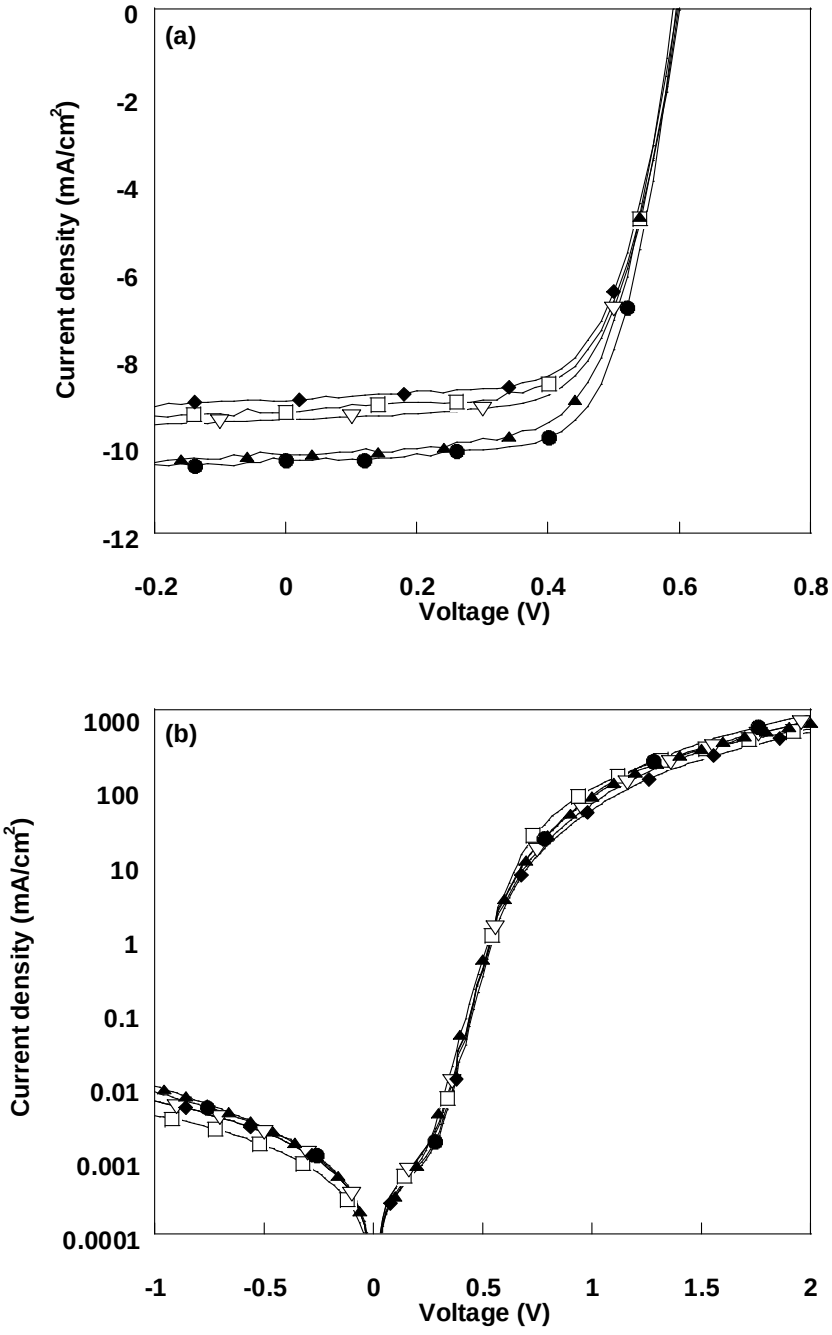

Figure 1. J-V curves of PV cells based on P3HT:PCBM with (□) 30 nm PEDOT:PSS, (□) 10 nm PEDOT:PSS, (□) 26 nm SPDPA, (▲) 14 nm SPDPA and (●) 10 nm SPDPA (a) under AM 1.5 (100mW/cm^2) illumination and (b) under dark.

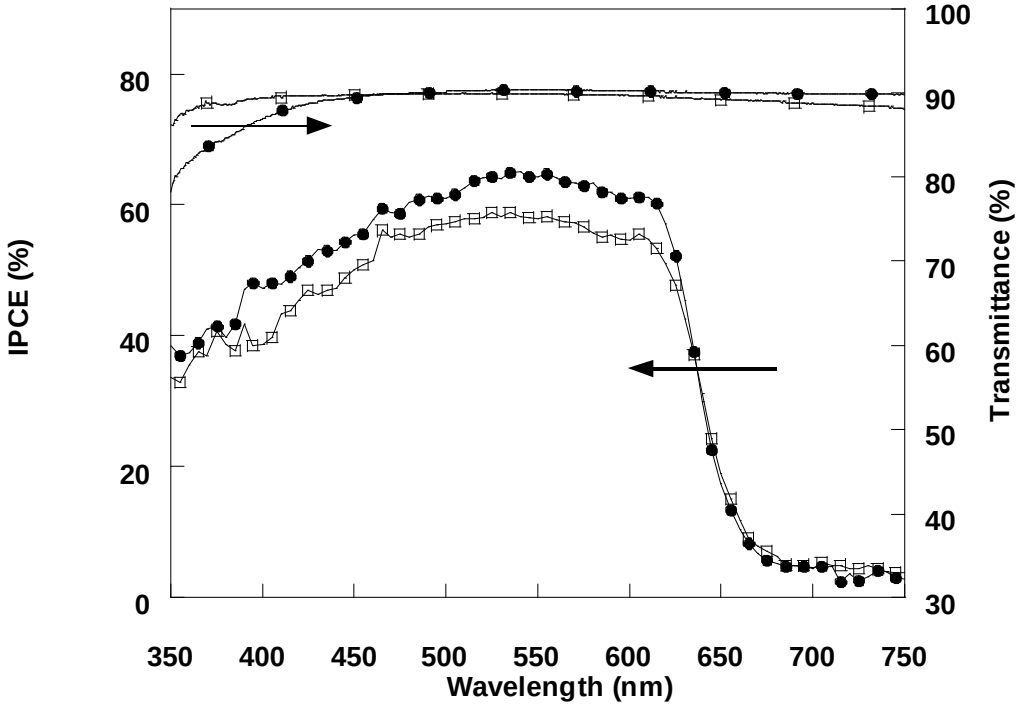

Figure 2. IPCE spectra for PV cells with PEDOT:PSS (□) and SPDPA (●); transmittance spectra of PEDOT:PSS (□) and SPDPA coated on ITO(●).

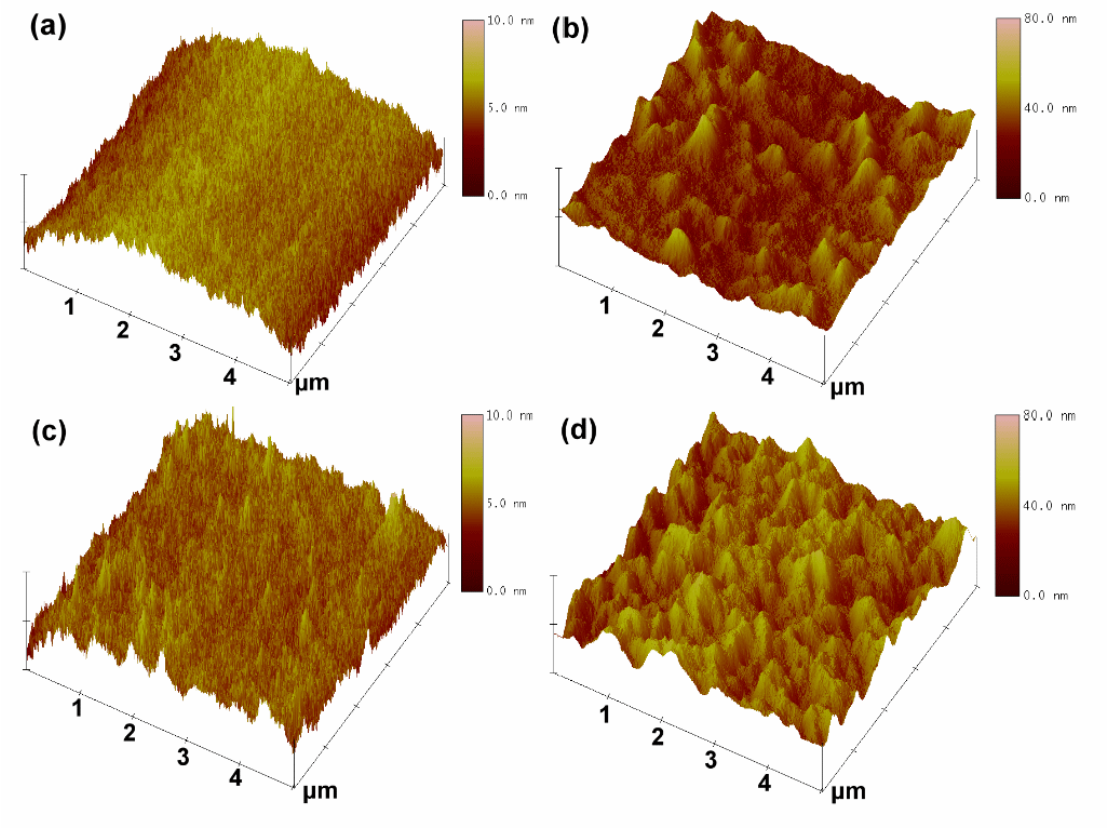

Figure 3. AFM images of P3HT:PCBM deposited on (a) the PEDOT:PSS through fast-grown film; (b) the PEDOT:PSS through slow-grown film; (c) the SPDPA through fast-grown film; (d) the SPDPA through slow-grown film

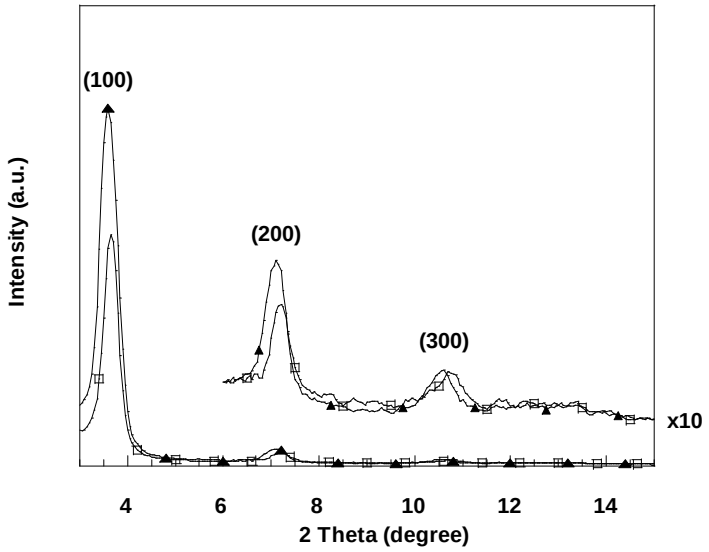

Figure 4. GI-XRD spectra of P3HT:PCBM slow-grown film onto the ITO/PEDOT: PSS (□) and ITO/SPDPA (▲) substrate.

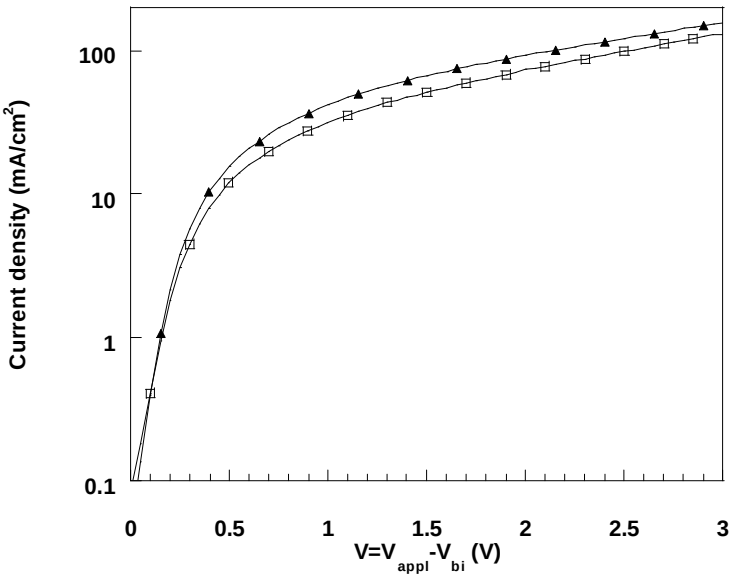

Figure 5. J-V curves for hole-only devices based on P3HT:PCBM slow-grown film with various hole collecting layers: PEDOT (□) and SPDPA at 3500 rpm (▲). We correct the applied voltage (V_{appl}) with build-in voltage (V_{bi}). The V_{bi} value is 0.1 V. The thicknesses of polymer films including HCL layer and active layer are 220 nm for PEDOT:PSS and 206 nm for SPDPA.

(a)

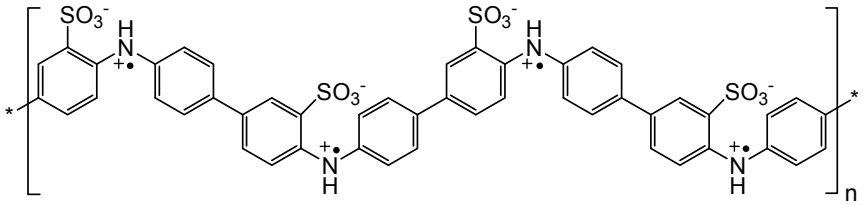

SPDPA

(b)

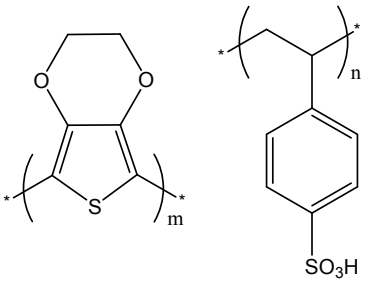

PEDOT:PSS

Scheme 1. The molecular structures for the hole collecting layer for this work.

VI. Future work

- Summarize and continue on the work of applying organic oxide/Al complex electrode for the high-performance BHJ solar cells.
- Apply SPDPA and organic oxide/Al complex electrode for the fabrication of inverted-type and environmentally stable polymer BHJ solar cells.
- Depth-profile measurement of X-ray photoelectron spectroscopy will be used to *in-situ* characterize the unique carbon-metal properties at the cathode interface.
- Development of the novel Al-C nano-composite materials.

VII. Conclusions

We had presented the fundamental studies on the polymer/metal junctions of HY-PPV-based PLEDs with and without introducing the organic-oxide buffer layer by the high-resolution XPS. The formation of an ultra-thin Al-C interlayer is verified in our research during the vacuum thermal deposition process of Al layer. The specific organic oxide/Al complex effectively facilitates the injection of electrons and also suppresses the formation of metal-induced EL quenching sites in the light-emissive polymer layer. The use of the organic oxide/Al cathode improves the EL intensity and luminous efficiency of HY-PPV-based PLED by approximately two orders of magnitude over those when Al is used as the device cathode. In addition, we had successfully applied SPDPA as HCL in fabricating high-performance polymer PV cells. The SPDPA has the function to increase the crystallinity of P3HT; to enhance the hole mobility; to reduce the series resistance; and to generate an Ohmic contact between HCL and P3HT. At current stage, PCE of 4.2%, FF of 0.68, and IPCE of 65.2% are presented in our works.

The study of polymer BHJ solar cells is an important technology for the development of the light-weight, low-cost, flexible, alternative energy source. Improving the device performance through the interfacial modification is a new strategy. We will continue on the studies to apply the unique organic oxide/Al complex electrode and SPDPA modified electrode for the fabrication of high-performance polymer BHJ solar cell. There are three major tasks in the project funded by AOARD-08-4076 entitled "Fabrication of high-performance polymer bulk-heterojunction solar cells by the interfacial modifications" on going; **i)** The fundamental studies to fully understand the unique interfacial properties at the polymer/electrode junction on the enhanced PCE of polymer BHJ solar cells. **ii)** The fabrication of inverted, multiple-junction polymer BHJ solar cells

by applying the newly synthesized sulfonated poly(diphenylamine) (SPDPA) as an effective junction buffer layer. The organic oxide/Al and SPDPA modified electrodes will be integrated for the fabrication of inverted-type and environmentally stable polymer BHJ solar cells. **iii)** The studies of the novel and giant magneto photo-conductance effect on polymer photovoltaic cells made of intrinsically non-magnetic organic components. The photovoltaic effect of the polymer BHJ solar can be modulated by the applied magnetic field, which could become a study for the novel type of energy source.